Received: 2 August 2021 | Revised: 5 October 2021 | Accepted: 5 October 2021

DOI: 10.1111/jace.18186

Journal of the American Ceramic Society

RESEARCH ARTICLE

Influence of Zn^{2+} doping on the morphotropic phase boundary in lead-free piezoelectric $(1-x)Na_{1/2}Bi_{1/2}TiO_3$-$xBaTiO_3$

Daniel Bremecker | **K. V. Lalitha** | **Siegfried Teuber** | **Jurij Koruza** | **Jürgen Rödel**

Division of Nonmetallic-Inorganic Materials, Department of Materials and Earth Sciences, Technical University of Darmstadt, Darmstadt, Germany

Correspondence
Daniel Bremecker, Division of Nonmetallic-Inorganic Materials, Department of Materials and Earth Sciences, Technical University of Darmstadt, 64287 Darmstadt, Germany.
EMail: bremecker@ceramics.tu-darmstadt.de

Funding information
Bundesministerium für Bildung und Forschung through project, Grant/Award Number: 13XP5091B; Deutsche Forschungsgemeinschaft under Grant Nr, Grant/Award Number: 414073759; Deutsche Forschungsgemeinschaft under, Grant/Award Number: KO 5948/1-1; TECHNISCHE UNIVERSITAET DARMSTADT

Abstract

A series of morphotropic phase boundary (MPB) compositions of (1–x) $Na_{1/2}Bi_{1/2}TiO_3$-x$BaTiO_3$ (x = 0.05, 0.055, 0.06, 0.065, 0.07), with and without 0.5 mol% Zn-doping was synthesized using the solid-state route. The samples were characterized using X-ray diffraction, dielectric analysis, and electromechanical measurements (piezoelectric d_{33} coefficient, coupling factor k_p, mechanical quality factor Q_m, and internal bias field E_{bias}). The increase in the ferroelectric-relaxor transition temperature upon Zn-doping was accompanied by a shift of the MPB toward the $Na_{1/2}Bi_{1/2}TiO_3$-rich side of the phase diagram. Higher tetragonal phase fraction and increased tetragonal distortion were noted for Zn-doped $(1-x)Na_{1/2}Bi_{1/2}TiO_3$-$xBaTiO_3$. In addition, ferroelectric hardening and the presence of an internal bias field (E_{bias}) were observed for all doped compositions. The piezoelectric constant d_{33} and the coupling coefficient k_p decreased by up to ~30%, while a 4- to 6-fold increase in Q_m was observed for the doped compositions. Apart from establishing a structure–property correlation, these results highlight the chemically induced shift of the phase diagram upon doping, which is a crucial factor in material selection for optimal performance and commercialization.

KEYWORDS
lead-free, morphotropic phase boundary, Na1/2Bi1/2TiO3-xBaTiO3, piezoceramic, Zn-doping

1 | INTRODUCTION

$Pb(Zr_{1-x}Ti_x)O_3$ (PZT) ceramics are widely used for piezoelectric applications in a broad range of sectors.[1] Lead is toxic and has been driven out of the marketplace for many applications like soldering, paint, plumbing and automotive fuel additives. In the future, the restrictions are likely to extend to certain piezoceramic products, which are mainly based on PZT. Piezoceramics are currently exempted from the Restriction of Hazardous Substances (RoHS).[2] However, the search for lead-free substitutes has become a major topic in ceramics research over the past decades and has established the research field of lead-free piezoceramics, with first prototypes and products (e.g.,

ultrasonic imaging probe, knocking sensor) emerging on the market.[3–6]

Bismuth-based solid solutions such as the (1–x)($Na_{1/2}Bi_{1/2}TiO_3$)-$xBaTiO_3$ (NBT-BT) system,[7] are promising candidates to replace PZT ceramics in certain application fields, for example, as sensors and resonators.[3] NBT-BT exhibits a morphotropic phase boundary (MPB) between rhombohedral and tetragonal symmetries and a complex local structure.[8–11] The compositions in the region of the MPB are nonergodic relaxors below the transition temperature, $T_{F\text{-}R}$.[12] An irreversible phase transition from the relaxor to the ferroelectric state is caused in these compositions upon application of external electric field.[10] This is accompanied by a change in oxygen octahedral tilting and a volume expansion of the unit cell.[13,14] At the MPB, the crystal structure changes from rhombohedral to tetragonal with increasing BT content, which is accompanied by a peak in properties, for example, a maximum in the piezoelectric constant d_{33}. The transition was reported to be positioned between NBT-6BT and NBT-7BT, and the inconsistency in the criticality can be assigned to different processing conditions and the resulting small deviations in stoichiometry and microstructure.[7,8,15,16] While the MPB compositions exhibit the highest piezoelectric and coupling coefficients, their lower depolarization temperature is a limiting drawback in applications demanding higher operational temperatures.[11,17,18]

NBT-BT has distinct advantages when contrasted to PZT. Tou et al.,[19] Doshida et al.,[20] and Hejazi et al.[21] demonstrated that NBT-based materials can withstand high vibration velocity and even outperform PZT-based materials. PZT-based materials suffer from a decreasing mechanical quality factor Q_m at high vibration velocities. This results in a nonlinear temperature increase of the ceramic, when operated at these velocities.[22–24] Certain applications such as high-power ultrasonics demand compositions with high mechanical quality factors. Ferroelectric hardening is a common approach to increase the mechanical quality factor of piezoelectric materials and several concepts have been reported to harden the NBT-BT system. Methods using point defects include Bi- or Na- nonstochiometry[25] and acceptor doping with Fe,[26–28] Co,[29] or Zn^{2+},[30] which modify the material on the atomic level. In comparison, second phase hardening approach involves using nonferroelectric, second phase particles in the matrix that constrain the domain wall mobility.[31,32]

Zn-doping in NBT-based materials not only leads to ferroelectric hardening, but also delays the thermal depolarization. Li et al.[17] discussed the effect of acceptor Zn-doping on the depolarization behavior of NBT-BT. It was suggested that the larger ionic radii and polarizability lead to an increased dipole moment in the BO_6 octahedron, suppressing the relaxor behavior by stabilizing the neighboring octahedron. Kodumudi Venkataraman et al.[30] observed stabilization of the tetragonal phase and a lower cubic phase fraction in Zn-doped NBT-6BT and NBT-9BT. Besides, the thermal stability of the electromechanical parameters of differently hardened NBT-6BT compositions has recently been reported.[33]

However, the influence of doping on the phase stability is poorly understood. The tetragonal and rhombohedral compositions of NBT-BT exhibit higher T_d than the MPB compositions. While this is a common feature noted for most MPB systems, the onset of a tetragonal distortion upon Zn-doping in a predominantly rhombohedral composition NBT-6BT indicates a shift of the MPB upon doping. In this work, we investigate the influence of Zn-doping on the crystallographic structure and electromechanical properties of a series of NBT-BT compositions across the MPB. Concurrently, the ensuing electromechanical property profile was related to the acceptor-doping modified morphotropic phase boundary, augmented with an additional focus on hardening behavior. As a result, the delay in the ferroelectric to relaxor phase transition is ascribed to the altered MPB upon acceptor Zn-doping.

2 | EXPERIMENTAL

(1–x)$Na_{1/2}Bi_{1/2}TiO_3$-$xBaTiO_3$ ceramics with $x = 0.05$, 0.055, 0.06, 0.065, 0.07 and with 0.5 mol% Zn substituted on the Ti-site were prepared by solid-state synthesis. These samples will be marked as NBT-5BT, NBT-5.5BT, NBT-6BT, NBT-6.5BT, NBT-7BT, NBT-5BT-0.5 Zn, NBT-5.5BT-0.5 Zn, NBT-6BT-0.5 Zn, NBT-6.5BT-0.5 Zn, NBT-7BT-0.5 Zn, respectively. Powders with given purities were utilized: Na_2CO_3 (99.5%), $BaCO_3$ (99.8%), Bi_2O_3 (99.975%), TiO_2 (99.6%), and ZnO (99.99%) (all from Alfa Aesar GmbH & Co. KG, Germany). Some of the processing conditions for the undoped and doped compositions were different, which is in the following indicated in parentheses. After weighing, powders were milled with yttria-stabilized zirconia balls in ethanol for 24 h at 250 rpm (doped: 6 h, 250 rpm), then dried and homogenized, and finally calcined at 900°C for 3 h using a heating rate of 5°C/min. Milling was subsequently repeated under the same conditions and was followed by another drying step. Cylindrical samples of either 10 or 15 mm in diameter were pressed at a uniaxial pressure of 40 MPa followed by a hydrostatic pressure of 200–350 MPa. The samples were placed in a closed alumina crucible with sacrificial powder and were sintered at 1150°C for 3 h using a ramp rate of 5°C/min (doped: 1100°C, 1 h, 5°C/min). The densified samples were then ground to a thickness of 0.7–0.8 mm. Silver electrodes were sputtered on the surfaces for electrical measurements after annealing at 400°C for 60 min to relieve the

residual stresses introduced by machining. Poling was done at 6 kV/mm for 15 min at 30°C.

Polished samples were thermally etched at 900°C for 10 min for grain size analysis. Pictures were taken with a scanning electron microscope (Philips XL30FEG, Amsterdam, the Netherlands). The three-dimensional average grain diameter was calculated from a minimum of 150 grains per composition with a numerical multiplication factor of 1.56 by assuming an isometric grain shape.[34] X-ray diffraction (XRD) was conducted on powder samples, prepared by crushing and annealing the sintered pellets. A Guinier diffractometer (Guinier-Camera G670, Guinier-Monochromator 611, X-Huber diffraction and positioning equipment) and a Cu-source with a monochromator (Cu Kα_1 $\lambda = 1.5409$ Å) were utilized in transmission geometry. Rietveld refinement was performed using Bruker's TOPAS software. Instrumental parameters were obtained by refining a standard silicon sample (NIST SRM640e) mixed with the sample powder. In the refinements, the Bragg peaks were modeled using the Thompson–Cox–Hastings pseudo-Voigt function.

Electromechanical properties were evaluated on at least three samples and error bars provided. The transition temperature from the ferroelectric to the relaxor state ($T_{F\text{-}R}$) was evaluated from temperature-dependent permittivity measurements of poled samples, performed at a heating rate of 2°C/min (Impedance Analyzer 4192A LF, HewlettPackard). The piezoelectric coefficient was determined using a Berlincourt-type d_{33}-meter (PM300, Piezotest). Mechanical quality factor and coupling coefficient were quantified using the resonance method with an impedance analyzer (Alpha-Analyzer, Novocontrol) according to the European standard EN 50324-2. The polarization and strain hysteresis were obtained from unpoled/unaged and poled/aged samples using a modified Sawyer–Tower circuit and an optical displacement sensor. The samples were aged by short-circuiting with an aluminum foil for one week after poling. The internal bias field (E_{bias}) was evaluated from strain hysteresis loops obtained with a triangular electric field of 6 kV/mm at 1 Hz.

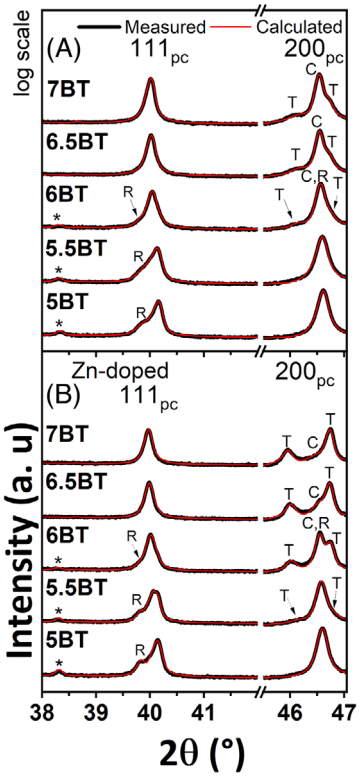

FIGURE 1 Observed (black) and calculated (red) X-ray diffraction profiles of 111 pc and 200 pc reflections for undoped NBT-BT (A) and NBT-BT- 0.5 mol% Zn-doped samples (B). The superlattice reflections are marked by an asterisk. "R" tags the split in 111 pc peak corresponding to rhombohedral distortion, while "T" tags the tetragonal distortion (002 and 200 tetragonal peaks in 200 pc)

3 | RESULTS

The sintered samples had a relative density of 94–97%. Undoped samples feature an average grain size of 1.2–2.1 μm, while Zn-doped samples show an average grain size of 9.4–15.6 μm. (Table S1). Representative microstructures with the highest/lowest BT content are provided in Figure S1. All samples exhibit a single-phase perovskite structure (Figures S2 and S3). The 111 pc and 200 pc reflections of all undoped NBT-BT diffraction profiles are highlighted in Figure 1. A superlattice reflection is present in NBT-5BT and NBT-5.5BT at about 38.3°, marked by the asterisk. 200 pc is a singlet and 111 pc has a shoulder on the lower 2θ side, indicating rhombohedral *R*3*c* symmetry.[35] This shoulder is tagged with R (R = rhombohedral). However, the diffractograms do not reveal a pure rhombohedral phase. Data can be best fitted when an additional cubic phase $Pm\bar{3}m$ is considered, which was previously reported to be the second phase besides *R*3*c* in these compositions.[36] On the other hand, the NBT-6BT is fitted with an additional tetragonal *P*4*mm* phase, due to the splitting of 200 pc peak at about 46°. This split caused by the tetragonal phase can be seen by a 002 peak marked with T (T = tetragonal) in Figure 1A as well as a shoulder on the right side of the 200 pc peak tagged with T as well. The main peak of the 200 pc reflex is caused by the cubic phase. No superlattice reflection is found in compositions from NBT-6BT to NBT-7BT. The peak splitting in 200 pc is more pronounced in NBT-6.5BT and NBT-7BT, while 111 pc peak splitting is absent. Thus, no rhombohedral phase is detected in NBT-6.5BT and NBT-7BT. The latter compositions can be

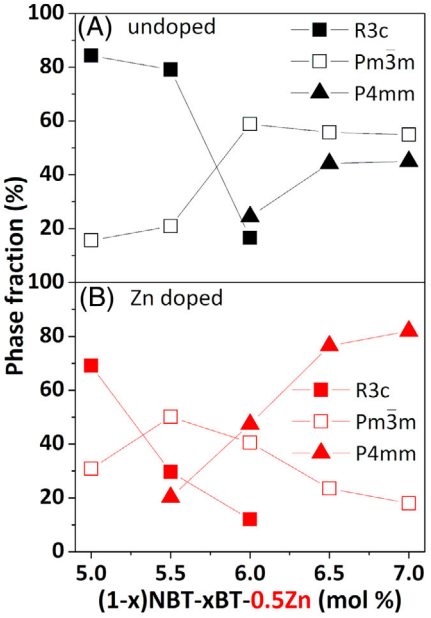

FIGURE 2 Evolving phase fractions across the morphotropic phase boundary in undoped (A) and Zn^{2+}-doped (B) NBT-BT

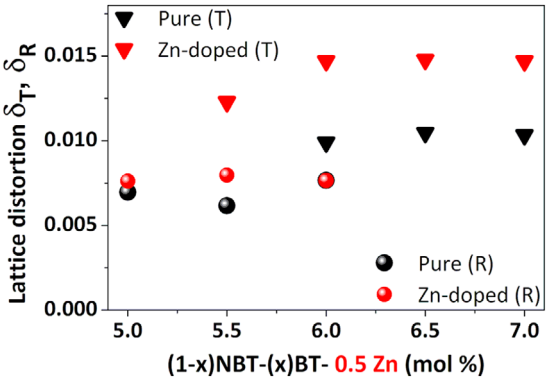

FIGURE 3 Lattice distortion of the tetragonal phase *P4mm* (δ_T, triangles) and the rhombohedral phase *R3c* (δ_R, circles) in undoped (black) and doped (red) NBT-BT (unpoled powder)

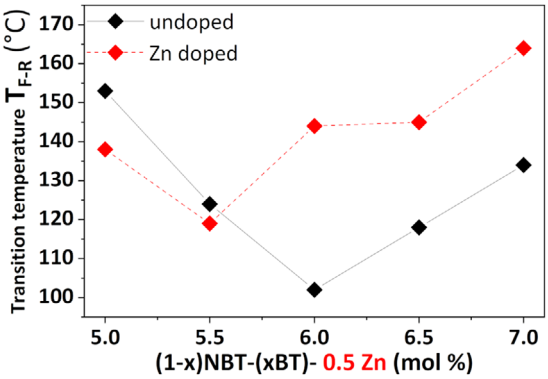

FIGURE 4 Transition temperature $T_{F\text{-}R}$ from ferroelectric to relaxor state in poled samples of undoped (black) and Zn-doped (red) NBT-BT. The corresponding permittivity versus temperature plots of all samples in poled and unpoled state can be found in the supplemental material from Figures S4 to S7

described by a mixture of tetragonal and cubic phases, as previously reported in the literature.[7,16,37]

Figures 1B and 2B display the observed X-ray patterns and refinement results for Zn-doped NBT-BT compositions. The diffractograms of NBT-5BT-0.5 Zn to NBT-6BT-0.5 Zn exhibit a distinct shoulder tagged with R (R = rhombohedral) on the lower 2θ side of the 111 pc peak, which becomes smaller with increasing BT content. The superlattice reflection at about 38.3° indicates the rhombohedral phase *R3c* marked by an asterisk. However, the 200 pc peak in NBT-5.5BT-0.5 Zn is broader and asymmetric in comparison to the undoped counterpart. This suggests the presence of a tetragonal phase already in NBT-5.5BT-0.5 Zn. For higher BT content, splitting of the 200 pc peak becomes more pronounced in comparison to the undoped material. Again the splitting caused by the tetragonal phase is marked by T (T = tetragonal) in Figure 1B. Both, the tetragonal phase fraction and the tetragonal lattice distortion are higher in the Zn-doped compositions. In contrast, the cubic peak becomes smaller, indicating a lower cubic phase fraction compared to the undoped samples.

Figures 2A and 2B provide the phase fractions obtained from Rietveld refinement for the undoped and doped NBT-BT compositions, respectively. In the undoped state, a decrease and eventual disappearance of the rhombohedral phase fraction is evidenced with increasing BT. The onset of the tetragonal phase occurs at NBT-6BT and increases with increasing BT content. The amount of the cubic phase is about 20% in NBT-5BT & NBT-5.5BT and rises to about 50–60% in the samples NBT-6BT to NBT-7BT.

Similar to undoped NBT-BT, the rhombohedral *R3c* phase is found up to 6 mol% BT for the doped compositions. However, the rhombohedral phase fraction is lower in the Zn^{2+}-doped compositions. An enhanced tetragonal phase fraction is found from NBT-5.5BT-0.5 Zn to NBT-7BT-0.5 Zn in the Zn-doped compositions. The cubic phase is found in all compositions. Compared to the undoped compositions, the cubic phase fraction in the doped state is higher for 5–5.5 mol% BT and lower for 6–7 mol% BT.

Figure 3 presents the tetragonal and rhombohedral lattice distortions as a measure for the noncubic distortion of the unpoled samples. The tetragonal lattice distortion δ_T is calculated from the c/a ratio,[38] while the rhombohedral lattice distortion δ_R is quantified from the lattice spacings d_{111} and $d_{11\text{-}1}$.[38] The strongest change in noncubic distortion is noted with an increase in δ_T from the MPB to the tetragonal side. Zn-doping alters the degree of lattice distortion to a large extent with about 30% on the tetragonal side. The enhancement in the tetragonal distortion of

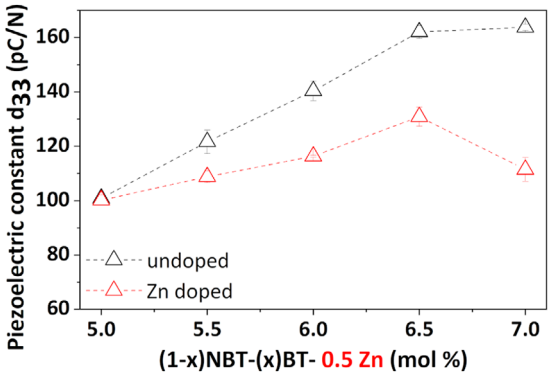

FIGURE 5 Piezoelectric charge constant d_{33} of undoped (black) and Zn^{2+}-doped (red) NBT-BT

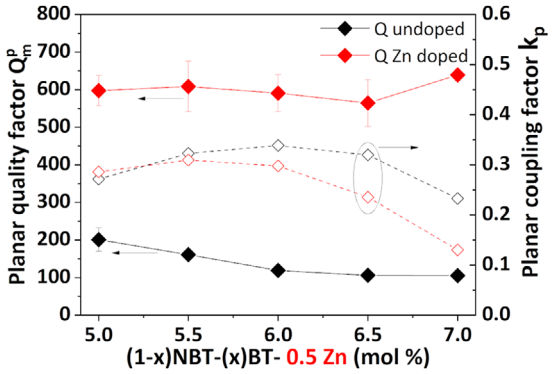

FIGURE 6 Planar coupling factor k_p (dotted) and planar mechanical quality factor Q_m^p (solid) of undoped (black) and doped (red) NBT-BT. Note that the error bars of k_p are smaller than the symbol size

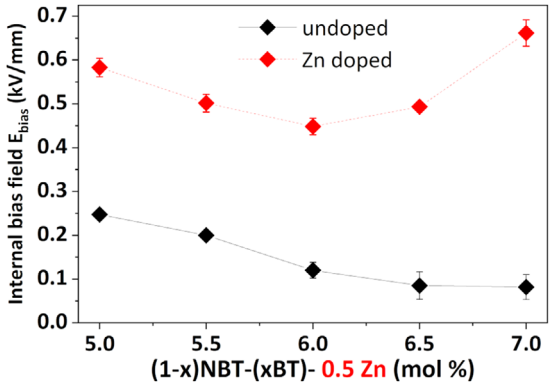

FIGURE 7 Internal bias field E_{bias} of undoped (black) and doped (red) NBT-BT

Zn-doped NBT-6BT is so drastic that it becomes comparable to that of NBT-9BT with attendant spontaneous transition from ergodic to nonergodic relaxor when cooling to room temperature.[30] A negligible increase in rhombohedral lattice distortion δ_R is noted for the doped samples in comparison to the undoped state.

For undoped NBT-BT, $T_{F\text{-}R}$ first decreases from NBT-5BT to NBT-6BT and then increases again for NBT-7BT. The minimum is located at NBT-6BT with a temperature of 103°C, in accordance with prior reports in literature.[15,39,40] When doped with Zn^{2+}, the basic trend of transition temperatures as a function of BT content is maintained; however, the position of the minimum is shifted to lower BT content (from NBT-6BT to NBT-5.5BT) and to higher temperatures with the minimum transition temperature increasing from 103°C (undoped) to 119°C (doped). The shift of transition temperature is stronger on the tetragonal side and smaller on the rhombohedral side. An increase in the depolarization temperature upon Zn-doping of NBT-6BT and NBT-9BT has also been reported previously.[17,30]

Figure 5 features the piezoelectric charge constant d_{33} for pure and Zn-doped NBT-BT. NBT-5BT exhibits the lowest value of 101 pC/N. The d_{33} increases with increasing the BT content and the maximum value of 164 pC/N is obtained for NBT-7BT. This is in agreement with other publications, such as Chen at al.[15] and Xu et al.[40] Upon Zn-doping, d_{33} increases from 100 pC/N (NBT-5BT-0.5 Zn) to 131 pC/N (NBT-6.5BT-0.5 Zn), but then decreases again to 111 pC/N (NBT-7BT-0.5 Zn). Comparison of the undoped and doped compositions reveals that Zn-doping leads to a decrease in the piezoelectric charge constant d_{33} in all compositions except for NBT-5BT-0.5 Zn. The decrease in d_{33} intensifies with increasing BT content.

Figure 6 highlights the large increase of the mechanical quality factor (Q_m^p) by a factor of three to six with Zn-doping. The reduction of the planar electromechanical coupling factor, k_p, depends on composition. In the case of pure NBT-BT, a small decrease in Q_m^p is observed from 201 for NBT-5BT to 105 for NBT-7BT. In contrast, the planar coupling factor k_p increases from NBT-5BT to NBT6BT and decreases again to NBT-7BT. Zn-doped compositions feature a large increase in Q_m^p (565–639). k_p increases from NBT-5BT-0.5 Zn to NBT-5.5BT-0.5 Zn and decreases again to NBT-7BT-0.5 Zn. k_p peaks for NBT-6BT and NBT-5.5BT-0.5 Zn.

The internal bias field (Figure 7), E_{bias}, of undoped NBT-BT drops from 0.25 kV/mm (NBT-5BT) to 0.08 kV/mm (NBT-7BT), which is in the range found in literature.[30] E_{bias} is strongly enhanced upon Zn-doping, with values between 0.45 and 0.66 kV/mm, and a noticeable minimum occurring at NBT-6BT.

4 | DISCUSSION

All the sintered samples exhibited a perovskite phase (Figures S2 and S3) and a high relative density, with Zn-doped compositions featuring larger average grain sizes (Figure S1). Kathua et al.[41] found that an increase in

grain size from 1 to 18 μm stabilizes the rhombohedral *R3c* phase. No clear trend could be observed in our samples, which may be related to smaller changes in the grain size. Therefore, we conclude that the changes in grain size in our compositions play a negligible role on the properties and are overshadowed by the Zn-doping effect.

The biggest change in crystallographic structure is the large increase in tetragonality after Zn-doping (Figure 3), which in turn widens the region of existence of the tetragonal phase and prompts a shift of the morphotropic phase boundary toward the rhombohedral side (Figure 2). This effect of Zn on tetragonality has been witnessed before in Bi-containing lead-free piezoceramics with $Bi(Zn,Ti)O_3$ exhibiting a giant tetragonality of 1.211.[42] As a consequence, $Bi(Zn,Ti)O_3$ has been employed as a modifier in other Bi-based lead-free piezoceramics in order to increase the Curie temperature (T_C), as well as alter the A- and B-site displacements.[43] Similar behavior has been observed by others for compositions such as NBT-6BT and NBT-9BT.[30] The correlation between noncubic distortion and phase transition temperature follows a common trend for Bi-based[40] as well as Pb-based piezoceramics.[44] A particular stabilization of one of the neighboring MPB crystal structures has also been reported before to shift the MPB in other systems.[44,45]

From the XRD refinement for undoped NBT-BT, it can be concluded that there is a gradual transition from the rhombohedral phase to the tetragonal phase with a larger unit cell across the MPB (Table S2). In this case, it appears that a larger B-site ion could have a similar effect to a larger A-site ion. This is substantiated by the shift of the MPB to smaller BT contents when doped with Zn.

The transition temperature from the ferroelectric poled state to the relaxor state ($T_{F\text{-}R}$) depicted in Figure 4 governs the depolarization temperature T_d, but may differ for materials where thermal fluctuations lead to randomization of the domain orientation already in the ferroelectric phase. In this instance, the depolarization temperature may be smaller than the phase transition temperature by about 10°C.[46] The enhanced stability of the ferroelectric phase and the shift of the MPB with Zn-doping are mimicked in the property profile of the investigated compositions. For example, the observed minimum in the transition temperature $T_{F\text{-}R}$ shifts from 6BT to 5.5BT and increases by 16°C upon addition of 0.5 mol% Zn (Figure 4). Piezoceramics often feature a maximum in the piezoelectric constant on the tetragonal side of the MPB.[47,48] In a similar fashion, the maximum in d_{33} is shifted by 0.5 mol% BT to the tetragonal side. The maximum in d_{33} is noted at 6.5 and 7 mol% BT in the undoped material and at 6.5 mol% BT for the Zn-doped material. k_p peaks at NBT-6BT for the undoped state and upon doping, this peak shifts to NBT-5.5BT-0.5 Zn. This is expected, due to the well-known proportionality between k_p and d_{33}.[49]

The piezoelectric activity and depolarization temperature are related to the changes in phase composition and crystallographic structure. In PZT, high piezoelectric activity around the MPB is attributed to a flattening of the free energy landscape,[50] which facilitates polarization rotation. In the same way, a flattened free energy usually leads to a more cubic-like structure and a lower depolarization temperature.[51,52] The opposite happens for the tetragonal compositions of NBT-BT when doped with Zn. The cubic phase fraction decreases from NBT-6BT to NBT-7BT. An increase in depolarization temperature and a decrease in the piezoelectric coefficient are evident. Moreover, it has been shown that a larger c/a ratio hinders domain wall motion and reduces piezoelectric activity in a lead-free BT-based systems.[53] Luo et al.[54] have previously demonstrated an increase in T_d and a simultaneous decrease in d_{33} with increasing the c/a ratio for the NBT-BT system.

In addition to compositional changes, point defects can also affect the electromechanical properties. In the literature, ferroelectric hardening is mostly associated with charged defects and their interaction with domain walls and polarization. Zn in the form of Zn^{2+} with an ionic radius of 74 pm is expected to incorporate on the Ti^{4+} B-site of the lattice with ionic charge compensation by oxygen vacancy formation.[17,55] Note that although charge compensation via oxygen vacancy formation is assumed to be dominant in NBT-based materials, evaporation of bismuth or the change of Ti^{4+} to Ti^{3+} are also possible mechanisms for charge compensation. In doped systems, the pinning of domain walls and hence the reduction of domain wall mobility have been ascertained to be derived from three possible mechanisms: volume effect, domain wall effect, and interface effect.[24,56] This is usually evidenced by a shift in the polarization hysteresis loop along the electric field axis and can be quantified by the internal bias field E_{bias}.[57–59] A ferroelectrically hardened material is associated with reduced electromechanical losses,[56] which result in a higher mechanical quality factor.[31] Hence, the observed increased quality factor and internal bias field are a direct consequence of the charged mobile defects generated by Zn-doping. We note that a direct evidence for the existence of defect complexes has not been found yet in this material; therefore, it is not possible to clearly distinguish between the different mechanisms affecting the domain wall movement.

Additionally, the hardening mechanism can be influenced by the increase in grain size, since this can alter the domain size and change the probability of each hardening mechanism.[60] But it is not the scope of this work to

elaborate in detail on the specific hardening mechanism. It is suggested as an interesting research topic for the future.

It is worth noting that in pure NBT-BT, the quality factor decreases across the MPB, from the rhombohedral to the tetragonal side. The opposite behavior is seen in the PZT system around the MPB, while for compositions away from the MPB, the tetragonal samples exhibit a larger quality factor. The latter is rationalized by the higher coercive field in the tetragonal phase. A higher coercive field hinders domain wall movement and leads to lower loss.[61] A similar explanation could apply to the NBT-BT system with a higher coercive field of the rhombohedral compositions.[62] No clear trend can be seen for the mechanical quality factor for doped compositions; this could be related to the larger error bars in the mechanical quality factor of these compositions.

5 | CONCLUSION

In this work, we clarify the role of Zn acceptor doping on the enhanced ferroelectric to relaxor transition temperature as well as the accompanying hardening effect. Zn-doping is found to shift the morphotropic phase boundary toward the rhombohedral side of the phase diagram. In addition, the tetragonality increases when doped with Zn. These changes in crystal structure are reflected by a change in properties. Albeit the increase in $T_{F\text{-}R}$, the minimum in $T_{F\text{-}R}$ shifts toward lower BT content upon doping. Concurrently, the piezoelectric constant, d_{33} decreases and the maximum shifts by a corresponding amount of BT to the rhombohedral side. Ferroelectric hardening with Zn-doping is reflected by a threefold increase in the internal bias field, as well as an increase in the mechanical quality factor.

ACKNOWLEDGMENTS

The authors gratefully acknowledge financial support by the Bundesministerium für Bildung und Forschung through project number 13XP5091B. J.K. acknowledges the support by the Deutsche Forschungsgemeinschaft under Grant Nr. 414073759 (KO 5100/3-1). Lalitha K.V. acknowledges the Deutsche Forschungsgemeinschaft under grant no. KO 5948/1-1 (Nr. 414311761) for financial support. Daniel Bremecker thanks Andreas Wohninsland for helpful discussions.

Open access funding enabled and organized by Projekt DEAL.

CONFLICT OF INTEREST

No conflict of interest exists in the submission of this manuscript. The manuscript is approved by all authors for publication.

ORCID

Daniel Bremecker https://orcid.org/0000-0002-8045-025X
K. V. Lalitha https://orcid.org/0000-0002-4848-5436
Jurij Koruza https://orcid.org/0000-0002-0258-6709

REFERENCES

1. Uchino K. Ferroelectric devices. CRC Press; 2018.
2. Bell AJ, Deubzer O. Lead-free piezoelectrics—the environmental and regulatory issues. MRS Bull. 2018;43(8):581-7.
3. Rödel J, Webber KG, Dittmer R, Jo W, Kimura M, Damjanovic D. Transferring lead-free piezoelectric ceramics into application. J Eur Ceram Soc. 2015;35(6):1659-81.
4. Shrout TR, Zhang SJ. Lead-free piezoelectric ceramics: alternatives for PZT? J Electroceram. 2007;19(1):113-26.
5. Koruza J, Bell AJ, Frömling T, Webber KG, Wang K, Rödel J. Requirements for the transfer of lead-free piezoceramics into application. J Mater. 2018;4(1):13-26.
6. Shibata K, Wang R, Tou T, Koruza J. Applications of lead-free piezoelectric materials. MRS Bull. 2018;43(8):612-6.
7. Takenaka T, Maruyama K-i, Sakata K. (Bi1/2Na1/2)TiO3-BaTiO3 system for lead-free piezoelectric ceramics. Jpn J Appl Phys. 1991;30(9S):2236.
8. Jo W, Daniels JE, Jones JL, Tan X, Thomas PA, Damjanovic D, et al. Evolving morphotropic phase boundary in lead-free (Bi1/2Na1/2)TiO3–BaTiO3 piezoceramics. J Appl Phys. 2011;109(1):014110.
9. Khatua DK, Agarwal A, Kumar N, Ranjan R. Probing local structure of the morphotropic phase boundary composition of Na0.5Bi0.5TiO3–BaTiO3 using rare-earth photoluminescence as a technique. Acta Mater. 2018;145:429-36.
10. Ma C, Tan X. In situ transmission electron microscopy study on the phase transitionsin lead-free (1−x) (Bi1/2Na1/2) TiO3–xBaTiO3 ceramics. J Am Ceram Soc. 2011;94(11):4040-4.
11. Paterson AR, Nagata H, Tan X, Daniels JE, Hinterstein M, Ranjan R, et al. Relaxor-ferroelectric transitions: sodium bismuth titanate derivatives. MRS Bull. 2018;43(8):600-6.
12. Zhang Q, Zhao X, Sun R, Luo H. Crystal growth and electric properties of lead-free NBT-BT at compositions near the morphotropic phase boundary. Phys Status Solidi. 2011;208(5):1012-20.
13. Garg R, Rao BN, Senyshyn A, Krishna P, Ranjan R. Lead-free piezoelectric system (Na 0.5 Bi 0.5) TiO3-BaTiO3: Equilibrium structures and irreversible structural transformations driven by electric field and mechanical impact. Phys Rev B. 2013;88(1):014103.
14. Jo W, Rödel J. Electric-field-induced volume change and room temperature phase stability of (Bi1/2Na1/2)TiO3-x mol.% BaTiO3 piezoceramics. Appl Phys Lett. 2011;99(4):042901.
15. Chen M, Xu Q, Kim BH, Ahn BK, Ko JH, Kang WJ, et al. Structure and electrical properties of (Na0.5Bi0.5)1−xBaxTiO3 piezoelectric ceramics. J Eur Ceram Soc. 2008;28(4):843-9.
16. Ma C, Guo H, Beckman SP, Tan X. Creation and destruction of morphotropic phase boundaries through electrical poling: a case study of lead-free (Bi1/2Na1/2)TiO3−BaTiO3 piezoelectrics. Phys Rev Lett. 2012;109(10):107602.
17. Li L, Zhu M, Zhou K, Wei Q, Zheng M, Hou Y. Delayed thermal depolarization of Bi0.5Na0.5TiO3-BaTiO3 by doping

acceptor Zn^{2+} with large ionic polarizability. J Appl Phys. 2017;122(20):204104.

18. Yin J, Tao H, Zhang Y, Han J, Huang Y, Li Z, et al. Advances in tuning the "d33 ∝ 1/Td" bottleneck: simultaneously realizing large d33 and high Td in Bi0.5Na0.5TiO3-based relaxor ferroelectrics. J Mater Chem A. 2020;8(18):9209-17.
19. Tou T, Hamaguti Y, Maida Y, Yamamori H, Takahashi K, Terashima Y. Properties of (Bi0.5Na0.5)TiO3–BaTiO3–(Bi0.5Na0.5)(Mn1/3Nb2/3)O3 lead-free piezoelectric ceramics and its application to ultrasonic cleaner. Jpn J Appl Phys. 2009;48(7S):07GM3.
20. Doshida Y, Shimizu H, Mizuno Y, Itoh K, Hirose S, Tamura H. Nonlinear behavior and high-power properties of (Bi,Na,Ba)TiO3 and (Sr,Ca)2NaNb5O15 piezoelectric ceramics. Jpn J Appl Phys. 2011;50(9S2):09ND6.
21. Hejazi M, Taghaddos E, Gurdal E, Uchino K, Safari A. High power performance of manganese-doped BNT-based Pb-free piezoelectric ceramics. J Am Ceram Soc. 2014;97(10):3192-6.
22. Uchino K, Hirose S. Loss mechanisms in piezoelectrics: how to measure different losses separately. IEEE Trans Ultrason Ferroelectr Freq Control. 2001;48(1):307-21.
23. Takahashi S, Hirose S, Uchino K, Oh K-Y, editors. Electromechanical characteristics of lead-zirconate-titanate ceramics under vibration-level change. Proceedings of 1994 IEEE International Symposium on Applications of Ferroelectrics; 1994: IEEE.
24. Slabki M, Venkataraman LK, Checchia S, Fulanović L, Daniels J, Koruza J. Direct observation of domain wall motion and lattice strain dynamics in ferroelectrics under high-power resonance. Phys Rev B. 2021;103(17):174113.
25. Prasertpalichat S, Cann DP. Hardening in non-stoichiometric (1 − x) Bi0.5Na0.5TiO3–xBaTiO3 lead-free piezoelectric ceramics. J Mater Sci. 2015;51(1):476-86.
26. Sapper E, Dittmer R, Damjanovic D, Erdem E, Keeble DJ, Jo W, et al. Aging in the relaxor and ferroelectric state of Fe-doped (1-x)(Bi1/2Na1/2)TiO3-xBaTiO3 piezoelectric ceramics. J Appl Phys. 2014;116(10):104102.
27. Shi J, Tian W, Liu X, Fan H. Electric-field induced phase transition and fatigue behaviors of (Bi0.5+x/2Na0.5-x/2)0.94Ba0.06Ti1-xFexO3 ferroelectrics. J Am Ceram Soc. 2017;100(3):1080-90.
28. Steiner S, Seo IT, Ren P, Li M, Keeble DJ, Frömling T. The effect of Fe-acceptor doping on the electrical properties of Na1/2Bi1/2TiO3 and 0.94 (Na1/2Bi1/2) TiO3–0.06 BaTiO3. J Am Ceram Soc. 2019;102: 5295-304.
29. Xu Q, Chen M, Chen W, Liu H-X, Kim B-H, Ahn B-K. Effect of CoO additive on structure and electrical properties of (Na0.5Bi0.5)0.93Ba0.07TiO3 ceramics prepared by the citrate method. Acta Mater. 2008;56(3):642-50.
30. Kodumudi Venkataraman L, Zhu T, Salazar MP, Hofmann K, Waidha AI, Jaud J, et al. Thermal depolarization and electromechanical hardening in Zn^{2+}-doped Na1/2Bi1/2TiO3-BaTiO3. J Am Ceram Soc. 2020; 104(5):2201-12.
31. KV L, Riemer LM, Koruza J, Rödel J. Hardening of electromechanical properties in piezoceramics using a composite approach. Appl Phys Lett. 2017;111(2):022905.
32. Zhao C, Gao S, Yang T, Scherer M, Schultheiß J, Meier D, et al. Precipitation hardening in ferroelectric ceramics. Adv Mater. 2021;33(36):e2102421.
33. Slabki M, Venkataraman LK, Rojac T, Rödel J, Koruza J. Thermal stability of the electromechanical properties in acceptor-doped and composite-hardened (Na1/2Bi1/2)TiO3–BaTiO3 ferroelectrics. J Appl Phys. 2021;130(1):014101.
34. Mendelson MI. Average grain size in polycrystalline ceramics. J Am Ceram Soc. 1969;52(8):443-6.
35. Sundari SS, Kumar B, Dhanasekaran R, editors. Structural, dielectric, piezoelectric and ferroelectric characterization of NBT-BT lead-free piezoelectric ceramics. IOP Conference Series: Materials Science and Engineering. IOP Publishing; 2013.
36. McQuade RR, Dolgos MR. A review of the structure-property relationships in lead-free piezoelectric (1−x) Na0.5Bi0.5TiO3–(x)BaTiO3. J Solid State Chem. 2016;242:140-7.
37. Garg R, Rao BN, Senyshyn A, Krishna PSR, Ranjan R. Lead-free piezoelectric system $(Na_{0.5}Bi_{0.5})TiO_3$-$BaTiO_3$: equilibrium structures and irreversible structural transformations driven by electric field and mechanical impact. Phys Rev B. 2013;88(1):014103.
38. Uchida N, Ikeda T. Electrostriction in perovskite-type ferroelectric ceramics. Jpn J Appl Phys. 1967;6(9):1079.
39. Hiruma Y, Watanabe Y, Nagata H, Takenaka T, editors. Phase transition temperatures of divalent and trivalent ions substituted (Bi1/2Na1/2)TiO3 ceramics. Key Eng Mater. 2007;350:93–6.
40. Xu C, Lin D, Kwok KW. Structure, electrical properties and depolarization temperature of (Bi0.5Na0.5)TiO3–BaTiO3 lead-free piezoelectric ceramics. Solid State Sci. 2008;10(7):934-40.
41. Khatua DK, Mishra A, Kumar N, Adhikary GD, Shankar U, Majumdar B, et al. A coupled microstructural-structural mechanism governing thermal depolarization delay in Na0.5Bi0.5TiO3-based piezoelectrics. Acta Mater. 2019;179:49-60.
42. Suchomel MR, Fogg AM, Allix M, Niu H, Claridge JB, Rosseinsky MJ. Bi2ZnTiO6: a lead-free closed-shell polar perovskite with a calculated ionic polarization of 150 μC cm-2. Chem Mater. 2006;18(21):4987-9.
43. Nishikubo T, Ogata T, Venkataraman LK, Isaia D, Pan Z, Sakai Y, et al. Polarization-and strain-mediated control of negative thermal expansion and ferroelasticity in BiInO3–BiZn1/2Ti1/2O3. Chem Mater. 2021;33(4):1498-505.
44. Leist T, Jo W, Comyn T, Bell A, Rödel J. Shift in morphotropic phase boundary in La-doped BiFeO3–PbTiO3 piezoceramics. Japan J Appl Phys. 2009;48(12R):120205.
45. Anton E-M, Schmitt LA, Hinterstein M, Trodahl J, Kowalski B, Jo W, et al. Structure and temperature-dependent phase transitions of lead-free Bi1/2Na1/2TiO3-Bi1/2K1/2TiO3-K0.5Na0.5NbO3 piezoceramics. J Mater Res. 2012;27(19):2466.
46. Jo W, Daniels J, Damjanovic D, Kleemann W, Rödel J. Two-stage processes of electrically induced-ferroelectric to relaxor transition in 0.94(Bi1/2Na1/2)TiO3-0.06BaTiO3. Appl Phys Lett. 2013;102(19):192903.
47. Kungl H, Hoffmann MJ. Temperature dependence of poling strain and strain under high electric fields in LaSr-doped morphotropic PZT and its relation to changes in structural characteristics. Acta Mater. 2007;55(17):5780-91.
48. Budimir M, Damjanovic D, Setter N. Piezoelectric anisotropy–phase transition relations in perovskite single crystals. J Appl Phys. 2003;94(10):6753-61.
49. Standard EN 50324-2 Piezoelectric properties of ceramic materials and components—part 2: methods of measurement—low power. BS EN 50324-2:2002. p. 30.
50. Damjanovic D. Comments on origins of enhanced piezoelectric properties in ferroelectrics. IEEE Trans Ultrason Ferroelectr Freq Control. 2009;56(8):1574-85.

51. Liu G, Kong L, Hu Q, Zhang S. Diffused morphotropic phase boundary in relaxor-PbTiO3 crystals: high piezoelectricity with improved thermal stability. Appl Phys Rev. 2020;7(2):021405.
52. Damjanovic D. Contributions to the piezoelectric effect in ferroelectric single crystals and ceramics. J Am Ceram Soc. 2005;88(10):2663-76.
53. Tutuncu G, Li B, Bowman K, Jones JL. Domain wall motion and electromechanical strain in lead-free piezoelectrics: insight from the model system (1 −x) ba(zr0.2ti0.8)o3–x(ba0.7ca0.3)tio3 using in situ high-energy x-ray diffraction during application of electric fields. J Appl Phys. 2014;115(14):144104.
54. Luo H, Liu H, Deng S, Hu S, Wang L, Gao B, et al. Simultaneously enhancing piezoelectric performance and thermal depolarization in lead-free (bi,na)tio3-batio3 via introducing oxygen-defect perovskites. Acta Mater. 2021;208:116711.
55. Shannon RD. Revised effective ionic radii and systematic studies of interatomic distances in halides and chalcogenides. Acta Crystallogr Sect A: Cryst Phys, Diffract, Theor General Crystallography. 1976;32(5):751-67.
56. Genenko YA, Glaum J, Hoffmann MJ, Albe K. Mechanisms of aging and fatigue in ferroelectrics. Mater Sci Eng: B. 2015;192:52-82.
57. Carl K, Hardtl K. Electrical after-effects in Pb(Ti,Zr)O3 ceramics. Ferroelectrics. 1977;17(1):473-86.
58. Robels U, Arlt G. Domain wall clamping in ferroelectrics by orientation of defects. J Appl Phys. 1993;73(7):3454-60.
59. Jaffe B, Cook WR, Jaffe HL. Piezoelectric ceramics. London; New York: Academic Press; 1971: p. 271-80.
60. Li Z, Thong HC, Zhang YF, Xu Z, Zhou Z, Liu YX, et al. Defect engineering in lead zirconate titanate ferroelectric ceramic for enhanced electromechanical transducer efficiency. Adv Funct Mater. 2021;31(1):2005012.
61. Yamamoto T. Ferroelectric properties of the PbZrO3–PbTiO3 system. Japan J Appl Phys. 1996;35(9S):5104.
62. Venkataraman LK, Frömling T, Rödel J. Role of matrix phase and electric field gradient in Na1/2Bi1/2TiO3-BaTiO3: ZnO composites. J Materiom. 2021.

SUPPORTING INFORMATION

Additional supporting information may be found in the online version of the article at the publisher's website.

How to cite this article: Bremecker D, Lalitha KV, Teuber S, Koruza J, Rödel J. Influence of Zn^{2+} doping on the morphotropic phase boundary in lead-free piezoelectric $(1 - x)Na_{1/2}Bi_{1/2}TiO_3$-$xBaTiO_3$. J Am Ceram Soc. 2022;105:1232–1240. https://doi.org/10.1111/jace.18186